ELSEVIER

Chemical Physics 197 (1995) 389–404

Chemical Physics

A kinetic analysis of the primary charge separation in bacterial photosynthesis. Energy gaps and static heterogeneity

M. Bixon [a], Joshua Jortner [a], M.E. Michel-Beyerle [b]

[a] *School of Chemistry, Tel Aviv University, Tel Aviv 69978, Israel*

[b] *Lehrstuhl für Physikalische und Theoretische Chemie, Technische Universität München, Lichtenbergstrasse 4, D-85748 Garching, Germany*

Received 11 January 1995; in final form 18 April 1995

Abstract

We consider the energetics, the mechanism and the implications of static heterogeneity for the primary electron transfer (ET) from the electronically excited singlet state of the bacteriochlorophyll dimer ($^1P^*$) in the bacterial photosynthetic reaction center (RC) and some of its mutants. The energetics of the primary ET was inferred from an analysis of the experimental free energy relation (at $T = 300$ K) between the short-time decay rates of $^1P^*$ and the oxidation potentials of the dimer (P) for a series of single site "good" mutants, for which geometrical changes are minimized and perturbations of the prosthetic groups of the accessory bacteriochlorophyll (B) and of the bacteriopheophytin (H) by the mutants are minor. This analysis resulted in the reasonable value of $\lambda_1 = 800 \pm 250$ cm^{-1} for the (mutant invariant) medium reorganization energy and $\Delta G_1^0(N) = -480 \pm 180$ cm^{-1} for the energy gap for the native (N) RC. The low value of $\Delta G_1^0(N)$ implies that the dominant room temperature ET mechanism for the native RC involves sequential ET. Next, we have explored the effects of heterogeneity on the primary ET by model calculations for the parallel sequential-superexchange mechanism, which is subjected to Gaussian energy distributions of the energies of the P^+B^-H and P^+BH^- ion pair states (with a width parameter of $\sigma = 400$ cm^{-1}). The modelling of the heterogeneous kinetics by varying the (mean) energy gap ΔG_1 between P^+B^-H and $^1P^*$ was performed to elucidate the temporal decay of $^1P^*$ and the ET quantum yield in "good" mutants, to explore the gross feature of primary ET in a triple hydrogen bonded mutant and to characterize some of the temperature dependence of the primary ET. The most pronounced manifestations of heterogeneity within the native RC and its single site mutants ($\Delta G_1 = -900$ to 300 cm^{-1}) are the nonexponential temporal decay probabilities for $^1P^*$, which exhibit long-time tails, with heterogeneity effects being marked (in the classical limit) when $\sigma(\Delta G_1 + \lambda_1) > \lambda_1 k_B T$. When $\Delta G_1 \gg \sigma$ (i.e., $\Delta G_1 \geqslant 1000$ cm^{-1}), the relaxation rate of $^1P^*$ is slow, being dominated by the dimer internal conversion rate, with the effects of heterogeneity being less marked, as is the case for the triple hydrogen bond mutant. Regarding mechanistic issues, our kinetic modelling implies that at room temperature, primary ET in the native RC and its single site mutants is dominated by the sequential route and only the triple mutant exhibits a marked contribution of the superexchange route. At low temperature ($T = 20$ K), ET in the native RC is still dominated by the sequential route (with a small (i.e., $\sim 10\%$) superexchange contribution being manifested in its long-time decay), for single site mutants there is an interplay between sequential and superexchange routes, while superexchange dominates ET in the triple mutant. The heterogeneous parallel sequential-superexchange mechanism is of intrinsic significance to insure the stability of primary photosynthetic ET for different native and mutagenetically modified RCs over a broad temperature domain.

0301-0104/95/$09.50
SSDI 0301-0104(95)00168-9

1. Introduction

Although the structure [1–11] of the bacterial photosynthetic reaction center (RC) was first determined ten years ago [1], the basic issues which pertain to the dynamics and kinetics of the primary charge separation [12–16] are not yet elucidated. The major difficulty involved in the understanding of this central energy conversion process in photobiology is that it requires information on the energetics, electronic interactions and (intermolecular and intramolecular) nuclear dynamics, which cannot be readily inferred from the structural data in the ground electronic state. This situation reflects on the intrinsic limitations of the structure to infer on the electron transfer (ET) excited state dynamics. The outstanding problems in the understanding of the primary charge separation from $^1P^*$ to H across the A branch of the RC are:

(1) *Mechanisms.* All the mechanisms proposed for the primary ET attribute a special role to the accessory bacteriochlorophyll B, which may involve: (I) A one-step superexchange mechanism [17–26]. (II) Two-step ET with P^+B^-H as a real chemical intermediate [27–38]. (III) The parallel sequential-superexchange mechanism [39,40], which provides a unified scheme that includes both the unistep and the sequential mechanisms as limiting cases. On the experimental front evidence for the sequential mechanism II in the native (N) RC is obtained from the following room temperature data ($T = 296$–300 K): (1) The single lifetime $\tau_1 = 2.6$–3.5 ps for the decay of $^1P^*$ in conjunction with the two lifetimes $\tau_1 = 3.5 \pm 0.4$ ps and $\tau_2 = 1.1 \pm 0.4$ ps for the evolution of the ion pair P^+BH^- (and presumably of P^+B^-H) in *R.sphaeroides* [33–36]. (ii) The time evolution interrogated in the infrared (920–1040 nm) region, which presumably is due to P^+B^-H [37]. (iii) The kinetics of the modified RC by the bacteriopheophytin → pheophytin substitution [38] and the kinetic analysis for the bacteriopheophytin → bacteriochlorophyll replacement [40,41].

(2) *Energetic parameters.* The nature of the primary process is dominated by the (free) energy gap ΔG_1 of the ion pair state P^+B^-H relative to $^1P^*$. Estimates from molecular dynamic simulations of the RC [41–43] are intrinsically limited due to incomplete input information, e.g., the location of accessory water molecules, and intermolecular long-range interactions. Experimental data on the recombination of the ion pair P^+BH^- [44] resulted in $\Delta G_1 > -600$ cm^{-1}, while the kinetic data on ET in the chemically bacteriopheophytin → pheophytin modified RC resulted in $\Delta G_1 = -450$ cm^{-1} [38]. No definite experimental information on the reorganization energies λ_1 for the primary process are available. The reorganization energy for the ET incorporates all the "low frequency" modes ($\hbar\omega < k_BT$ at $T = 300$ K) which involve the intermolecular modes of the dimer and the protein modes. The analysis of the magnetic field effects on the recombination of the ion pair $P^+BH^- \rightarrow {}^3P^*$ results in the reorganization energy $\lambda_T > 1300$ cm^{-1} [45] for this process. The spectroscopic electron–medium phonon coupling for the electronic excitation $P \rightarrow {}^1P^*$ gives the spectroscopic reorganization energy $\lambda_S = 250$ cm^{-1} [46,47], which definitely constitutes a lower limit for the medium reorganization energy for the primary ET process (between $^1P^*$ and P^+B^-H or P^+BH^-). An analysis of the decay of $^1P^*$ of *R.capsulatus* and ten of its local L181 and M208 mutants, gives a surprisingly low value of $\lambda_1 \leqslant 250$ cm^{-1} at 295 K, which is even lower than λ_S [48].

(3) *Symmetry breaking.* The remarkable unidirectionality of the primary charge separation was attributed [21,23,39,41–43,49–51] to the cumulative contributions of the electronic coupling and of the nuclear Franck–Condon factor (originating from the change of the free energy gap between $^1P^*$ and P^+B^-H), with both classes of effects reinforcing the large branching ratio for ET across the A branch.

(4) *Kinetic heterogeneity.* Until a few years ago, the experimental ps and subps results for the kinetics of the primary charge separation process in the RC were interpreted in terms of single lifetimes for $^1P^*$ and the ion pairs [13–16]. This approach implied that inhomogeneous effects on the kinetics are minor. Indication for inhomogeneous kinetics were inferred from the dependence of the kinetics on the probing wavelength [52,53]. Recently, long-time tails were observed in the decay of $^1P^*$ as interrogated by stimulated emission and in fluorescence upconversion [36,48,54,55]. The decay of $^1P^*$ in the wild type reaction center could be fit by a biexponential with $\tau_1 = 2.6$ ps and $\tau_3 = 12$ ps with relative amplitudes of $A_3/A_1 \approx 0.15$ [36,48]. The biexponential

pattern prevails also for a variety of local mutants with A_3/A_1 being considerably larger. The most straightforward (though admittedly not exclusive) interpretation involves structural heterogeneity resulting in a continuous (or bimodal) distribution of the energy gaps and/or the reorganization energies and/or the electronic couplings. Experimental information on the energetic spread of the energy of the P^+BH^- ion pair state relative to $^1P^*$, which was accounted for in terms of a Gaussian distribution with a width parameter $\sigma = 400$ cm^{-1} (i.e., the FWHM being $2(2 \ln 2)^{1/2}\sigma$), was inferred from magnetic field effects on the recombination of the ion pair [56]. Concurrently, theoretical expressions were provided [48,57] for the ET rates in an inhomogeneously broadened (dispersive) system.

(5) *Vibrational coherence.* An oscillatory contribution to the stimulated decay of $^1P^*$ was exhibited [58–60] following fs excitation at low (10 K) and at room temperature, with a damping time of 0.6–0.8 ps and characteristic frequencies of 15–200 cm^{-1}. This pattern is attributed to vibrational coherence effects.

(6) *Vibrational relaxation.* The observation of vibrational coherence effects [58–60] indicates that vibrational relaxation within the initial $^1P^*$ manifold occurs on the time scale of the primary ET process. Nevertheless, for the case of activationless ET, as is the case here, the microscopic ET rates are insensitive to the details of the distribution of the initial vibrational states [61], and the ET dynamics is nearly invariant with respect to medium dynamics. This conclusion is supported by the experimental observation that the lifetime of the electronic origin of $^1P^*$ at 4.2 K inferred from hole burning [47] is the same as the time-resolved decay of $^1P^*$ [33–36,48].

This paper focuses on the analysis of the kinetics of the primary charge separation in the RC addressing the following issues:

(A) The phenomenological energetic parameters for the primary process, i.e., the energy gap ΔG_1^0 and the medium reorganization energy λ_1^0. This information will be extracted from a phenomenological analysis of the decay rates of $^1P^*$ in the native RC and in a series of single site mutants [36,48,62–64]. The energetics will provide a clue for the mechanism of the primary process.

(B) The exploration of the parallel sequential-superexchange mechanism [39] for the primary charge separation over a broad range of the energy gap ΔG_1 (Fig. 1) between $^1P^*$ and P^+B^-H. In our previous analysis [39] we considered this mechanism for the primary processes in the native RC. In view of our ignorance of ΔG_1 we have modified the electronic coupling for each value of this (free) energy gap, to reproduce the experimental ET times τ_1 and τ_2. In the present work we shall utilize the ΔG_1 value and the λ_1 value extracted for the native RC (point (A) above). Subsequently, the homogeneous kinetics will be investigated for a series of ΔG_1 values.

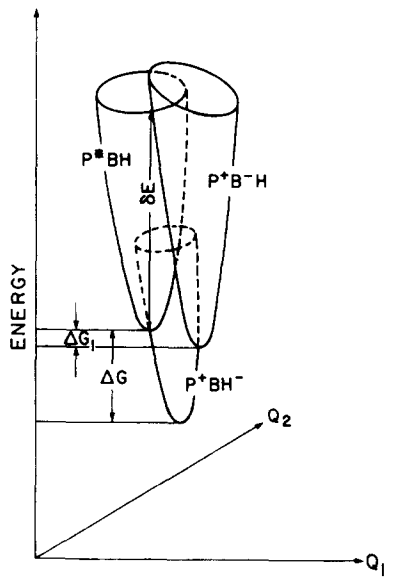

Fig. 1. Schematic potential energy surfaces for the primary charge separation in the RC.

(C) Kinetic modelling of the effects of static heterogeneity on the parallel sequential-superexchange mechanism. The foregoing analysis (B) has to be extended to incorporate the effects of inhomogeneous kinetics, whose implications on the nonexponential (dispersive) kinetics were explored. This analysis will provide information on the energy gap dependence of the (averaged) initial decay times and quantum yields for charge separation and of the branching ratios between the sequential and superexchange channels. This analysis will elucidate the gross features of the ET kinetics in a series of mutants [36,48,62–65] of the RC.

2. Energetic parameters for the primary process

We shall utilize a phenomenological analysis of the kinetics and energetics to extract the free energy gap ΔG_1^0 and the medium reorganization energy λ_1^0 of the charge separation process from $^1P^*$. In view of the current uncertainty in the primary process, the phenomenological parameters ΔG_1^0 and λ_1^0 may differ from ΔG_1 and λ_1, respectively. We have attempted to construct a free energy relationship for the primary ET using the following data for single site mutants [36,48,62–64,65]: (i) The kinetic data for the nonexponential decay of $^1P^*$. We have used the short-time decay component for the rate (denoted k_{ET}), with some justification of this heuristic treatment of heterogeneity which will be given in Section 4. (ii) The oxidation potentials $E_R(P^+/P)$ of P in the RCs. It is assumed that

$$\Delta G_1^0 = E_R(P^+/P) + B, \tag{2.1}$$

where B is a numerical constant. Eq. (2.1) implies that equal changes are induced by mutation in the redox potentials of $^1P^*/P^+$ and of P/P^+ and that the mutation solely perturbs P (and not B_A or H_A).

In Fig. 2 we portray the free energy dependence of ln k_{ET} versus $E(P^+/P)$ for single site mutants of

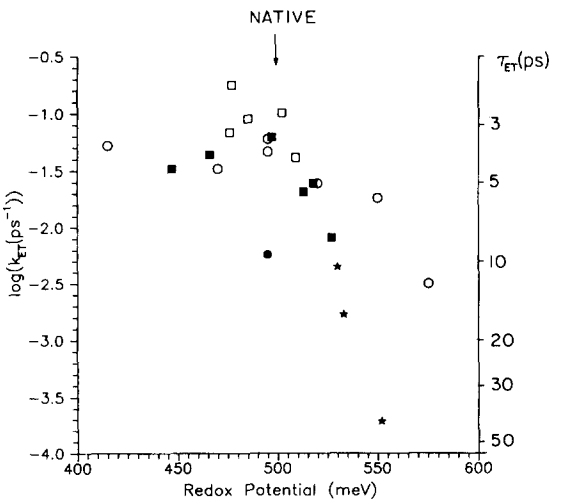

Fig. 2. The dependence of the experimental rates k_{ET} (and lifetimes $\tau_{ET} = k_{ET}^{-1}$) of the decay of $^1P^*$ for various single site mutants at room temperature, on the dimer redox potentials. The sources of the experimental data are: (■), (□) Ref. [48], (●) (○) Refs. [62,63], stars: Ref. [64].

R.capsulatus [48], and of *R.sphaeroides* [36,62–64]. The large spread of the data (Fig. 2) precludes the establishment of a free energy relationship. This failure reflects the inapplicability of Eq. (2.1) or/and the modification of other parameters, i.e., the electronic coupling V or λ_1^0 by site mutagenesis. A valid free energy relationship between ln k_{ET} and $E_R(P^+/P)$ is expected to be obeyed provided that the following constraints regarding geometry and interactions are satisfied:

(A) Minimization of geometrical changes which may modify V. Such changes will be induced by the replacement of the tyrosine (Y) M210 in *R.sphaeroides* (M208 in *R.capsulatus*) residue by a smaller (i.e., threonine, leucine or isoleucine) or by a bulkier (i.e., tryptophane (W)) residue. On the other hand, phenylalanine (F) and histidine (H) are closer to in size to Y, and H may even hydrogen bond like Y.

(B) Minimization of the perturbation of the prosthetic groups B_A and H_A by the mutations. All the site mutants of Y M210 (M208) [48,64] are excluded, and so is the GM203 → D (glycine (G) to aspartic acid (D)) mutant, which was specifically designed to affect B_A [62].

Guided by these empirical rules we have taken for the analysis of the free energy relation all the L181 mutants of the Chicago–Argonne group [48], the Y-Y mutant from the Munich group [36] and the relevant mutants from the Arizona group [62,63]. For the native RC we have taken the data for *R.capsulatus* [48], and *R.sphaeroides* [36,64]. These data are scattered (due to different samples and interrogation methods) by ±35%, providing a lower limit for the uncertainty of the experimental data.

The experimental k_{ET} data at $T = 295$ K for the native RC, together with those for the "good" mutants (obeying rules (A) and (B) above), fit nicely (Fig. 3) the theoretical free energy gap dependence

$$k_{ET} = (2\pi V^2/\hbar) F(\lambda_1^0, S_c, \hbar\omega_c, \Delta G_1^0, T), \tag{2.2}$$

where F is the nuclear Franck–Condon factor (see Section 3), which is characterized by low frequency modes with the reorganization energy λ_1^0 and by the high frequency mode ω_c with a coupling strength S_c. For the "good" mutants we implicitly assume that V and λ_1^0 are invariant and ΔG_1^0 is given by Eq. (2.1). At this stage we do not commit ourselves to

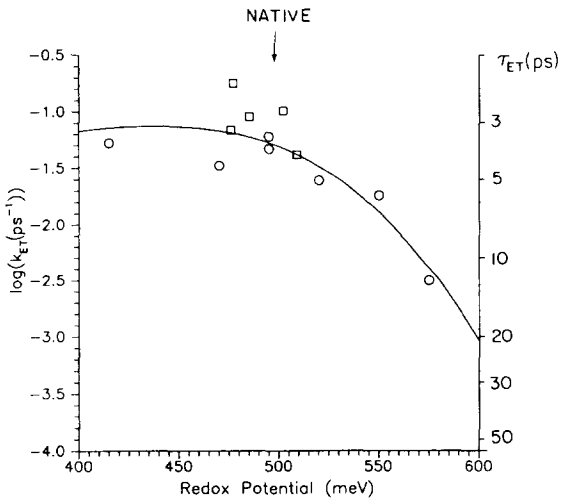

Fig. 3. Theoretical curve fitting of the free energy relationship for the experimental data of ln k_{ET} versus $E_R(P^+/P)$ for "good" mutants at room temperature (see text). The solid curve was calculated using the following parameters: Electronic couplings $V_{PB} = 20$ cm^{-1}; $V_{BH} = 40$ cm^{-1}. The reorganization energies are: $\lambda = 1600$ cm^{-1}; $\lambda_1 = 800$ cm^{-1}; $\lambda_2 = 800$ cm^{-1}. High frequency vibration: $\omega = 1500$ cm^{-1} with a shift of $S_c = 0.5$, low-frequency modes $\omega = 95$ cm^{-1}. Internal conversion rate of $^1P^*$ $k_d = 1/300$ ps^{-1}, recombination rate of P^+B^- $k_R = 1/1000$ ps^{-1}, and overall recombination rate of P^+BH^- $K_{R2} = 1/10000$ ps^{-1}. The experimental data are taken from: (○) Refs. [62,63] and (□) Ref. [48].

the nature of the charge separation from $^1P^*$, i.e., sequential or superexchange mechanism, although the simple form of (2.2) implies that one of these mechanisms dominates. The parameters λ_1^0 (which is taken to be mutant invariant) and ΔG_1^0 (which is mutant dependent according to Eq. (2.1)) will be determined from the analysis of the experimental data [36,48,62,63]. Good account of the free energy relationship for k_{ET} can be accomplished (Fig. 3) with the following parameters: (i) The medium reorganization energy $\lambda_1^0 = 800$ cm^{-1}. (ii) The uniform shift of the (free) energy scale, Eq. (2.1), is $B = -4500$ cm^{-1}. (iii) For the high frequency mode we have chosen the traditional values [39,66] $\hbar\omega_c = 1500$ cm^{-1} and $S_c = 0.5$. (iv) The electronic coupling is $V = 20$ cm^{-1}. From this analysis we infer that the energy gap for the native RC is $\Delta G_1^0(N) = -480$ cm^{-1}. In view of the spread of the experimental data (Fig. 3) the energetic parameters at room temperature, which provide an adequate fit of these results, are

$$\lambda_1^0 = 800 \pm 250 \text{ cm}^{-1}.$$

$$\Delta G_1^0(N) = -480 \pm 180 \text{ cm}^{-1}.$$

From these results we conclude that:

(1) The value of the reorganization energy λ_1^0 obtained herein is considerably higher than the surprisingly low value ($\lambda_1^0 \leqslant 250$ cm^{-1}), which was previously inferred from the analysis of single site mutants at $T = 295$ K [48]. Our value of λ_1^0 is lower than the value $\lambda_T > 1300$ cm^{-1} [45] and satisfies the constraint for the spectroscopic data $\lambda_1^0 > \lambda_S \approx 250$ cm^{-1} [46,47].

(2) The low value of $\Delta G_1^0(N) = -480 \pm 180$ cm^{-1} obtained herein for the native RC is considerably lower in its absolute value than the energy gap $\Delta G = -2000$ cm^{-1} between $^1P^*$ and P^+BH^- [67,68]. This result implies that the first ET step in the native RC at room temperature is not a direct superexchange mediated ET to H. The low value of $\Delta G_1^0(N)$ is in good agreement with the lower limit $\Delta G_1 > -600$ cm^{-1} previously inferred from the analysis of magnetic data for the P^+BH^- ion pair [44] and the value $\Delta G_1 = -450$ cm^{-1} derived from time-resolved data for the chemically modified RC [38]. Accordingly, the dominant room temperature mechanism for the native RC involves sequential ET, and we can identify $\Delta G_1^0(N) = \Delta G_1(N)$ (Fig. 1).

We have to be aware of some of the pitfalls in the present analysis. From the experimental point of view, we have utilized in Fig. 3 data for different samples from different laboratories, increasing the experimental uncertainty. In our analysis we have invoked the invariance $\lambda_1^0 = \lambda_1$ for different mutants. Furthermore, we have provided only a heuristic account of heterogeneity effects. This important issue will now be addressed for the primary ET.

3. The parallel sequential-superexchange mechanism

We proceed to provide model calculations for the kinetics of the primary ET in the native RC, and its mutants [36,48,62,63,65]. The kinetic scheme for the

parallel sequential-superexchange mechanism consists of [39,40]

(i) sequential route

$$^1P^*BH \underset{k_{-1}}{\overset{k_1}{\rightleftharpoons}} P^+B^-H \xrightarrow{k_2} P^+BH^-, \tag{3.1}$$

(ii) superexchange route

$$^1P^*BH \underset{k_-}{\overset{k}{\rightleftharpoons}} P^+BH^-, \tag{3.2}$$

(iii) quionone reduction

$$P^+BH^-Q \xrightarrow{k_Q} P^+BHQ^-, \tag{3.3}$$

(iv) internal conversion of dimer

$$^1P^*BH \xrightarrow{k_d} PBH, \tag{3.4}$$

(v) recombination of ion pairs

$$P^+B^-H \xrightarrow{k_R} PBH \tag{3.5}$$

$$P^+BH^- \xrightarrow{k_S} PBH \tag{3.6}$$

$$P^+BH^- \xrightarrow{k_T} {}^3P^*BH. \tag{3.7}$$

The theoretical description for the ET rates will be given in terms of the conventional multiphonon nonadiabatic theory, which expresses the ET rate in the form $k = (2\pi/\hbar)V^2F$, where V is the electronic coupling and F is the Franck–Condon factor. The validity conditions for the applicability of this simple scheme, which we recently discussed [40,61], are:

(1) The applicability of the nonadiabatic limit, which for characteristic parameters for the RC imply that [40] $V < 70\ \mathrm{cm}^{-1}$ at $T = 300$ K. This relation, which is inferred from an a posteriori analysis, is obeyed for the ultrafast ET process and for all the subsequent ET reactions in the RC.

(2) Insensitivity of the ET rates to medium dynamics. This state of affairs can be realized under two circumstances. (i) Fast medium relaxation dynamics. Our previous discussion [39,40] of molecular dynamics simulations for the temporal response of the RC to charge redistribution indicate that the condition of fast medium dynamics is on the verge of applicability for the ultrafast ps and subps primary rates. (ii) Activationless ET. We have recently demonstrated [61] that activationless ET cannot be described in terms of the diffusion towards a point sink at the intersection of the potential nuclear surface at the minimum of the initial nuclear surface (for the medium modes). Rather, for activationless ET the microscopic ET rates are insensitive (within a numerical factor of ~ 2) to the distribution of the initial vibrational states [61]. Accordingly, the (activationless) primary ET processes in the RC are not controlled by medium dynamics and can be reasonably well described in terms of the conventional ET rate from an equilibrated vibrational manifold. The four microscopic primary ET rate constants in Eqs. (3.1) and (3.2) are:

The superexchange rate

$$k = \frac{2\pi}{\hbar}(V_{PB}V_{BH}/\delta E)^2 \times F(\lambda, \omega_m, S_c, \hbar\omega_c, \Delta G, T). \tag{3.8}$$

The first sequential rate

$$k_1 = \frac{2\pi}{\hbar}V_{PB}^2 F(\lambda_1, \hbar\omega_m, S_c, \hbar\omega_c, \Delta G_1, T). \tag{3.9}$$

The reverse rate

$$k_{-1} = k_1 \exp(-\Delta G_1/k_B T). \tag{3.10}$$

The second sequential rate

$$k_2 = \frac{2\pi}{\hbar}V_{BH}^2 F(\lambda_2, \hbar\omega_m, S_c, \hbar\omega_c, \Delta G_2, T). \tag{3.11}$$

Here V_{PB} and V_{BH} are the electronic coupling terms between $^1P^*BH/P^+B^-H$ and P^+B^-H/P^+BH^-, respectively, and $\delta E = \Delta G_1 + \lambda_1$ is the vertical energy difference between the potential surfaces of $^1P^*BH$ and P^+B^-H at the minimum of the former (Fig. 1). ΔG, ΔG_1 and ΔG_2 are the (free) energy gaps. The medium vibrational modes are characterized by the average frequency ω_m and reorganization energies λ, λ_1 and λ_2. The high-frequency intramolecular vibrations are represented by a single effective vibrational mode ω_c and an effective reduced shift S_c. The Franck–Condon factors are

$$F(\lambda, \hbar\omega_m, S_c, \hbar\omega_c, \Delta G, T) = \sum_{n=0}^{\infty} F_m(\Delta G - n\hbar\omega_c)F_c(n), \tag{3.12}$$

with the medium contributions

$$F_m(\Delta E) = (\hbar\omega_m)^{-1}\left(\frac{\bar{v}+1}{\bar{v}}\right)^{p/2} \times \exp[-S_m(2\bar{v}+1)] \times I_p(2S_m[\bar{v}(\bar{v}+1)])^{1/2}, \quad (3.13)$$

where $\bar{v} = [\exp(\hbar\omega_m/k_BT)-1]^{-1}$ is the thermal population of the mode, $p = \Delta G/\hbar\omega_m$, $S_m = \lambda/\hbar\omega_m$ and $I_p(\cdot)$ is the modified Bessel function of order p. The intramolecular high-frequency contribution is

$$F_c(n) = \exp(-S_c)S_c^n/n!. \quad (3.14)$$

In the choice of the energetic and nuclear parameters, which determine the primary rates (3.8)–(3.10), we were guided by our previous mapping of the kinetic observables and by the energetic parameters inferred in Section 2 for the native RC. The following parameters were chosen:

(1) *Energy gaps.* The energy gaps ΔG_1 and ΔG_2 (Fig. 1) between $^1PB^*H$ and P^+B^-H and between P^+B^-H and P^+BH^-, respectively, are related by

$$\Delta G = \Delta G_1 + \Delta G_2. \quad (3.15)$$

For the native RC, $\Delta G = -2000\ cm^{-1}$ [67,68], $\Delta G_1 = -500\ cm^{-1}$ (Section 2) and $\Delta G_2 = -1500\ cm^{-1}$. For mutants, where the major perturbation is exerted on the dimer (Section 2), one expects that ΔG_2 is invariant, while ΔG_1 and ΔG are modified. The energy gap ΔG_1 was varied in the range $\Delta G_1 = -1000$ to $1500\ cm^{-1}$, which implies the variation of $\Delta G = -2500\ cm^{-1} - 0$.

(2) *Vibrational frequencies.* For the low frequency modes we have taken $\omega_m = 95\ cm^{-1}$ [39,66], which also corresponds to the weighted mean value of the low-frequency modes ($\sim 30\ cm^{-1}$ for the protein and $\sim 120\ cm^{-1}$ for the special pair) determined by Small et al. [47]. For the high-frequency mode we take $\omega_c = 1500\ cm^{-1}$ [39,66].

(3) *Nuclear reorganization energies.* For the rate k_1 in Eq. (3.1) we have taken the experimental estimate $\lambda_1 = 800\ cm^{-1}$ (Section 2). k_1 is nearly activationless in the native RC. λ_2 for k_2 in Eq. (3.2) is unknown and we took $\lambda_2 \approx \lambda_1$, i.e., $\lambda_2 = 800\ cm^{-1}$. The medium coupling strengths S_j ($j = 1, 2$) are $\lambda_j = S_j/\hbar\omega_1$. For k, Eq. (3.2), we took $\lambda = 1600\ cm^{-1}$ from the analysis of the P^+H^- radical pair dynamics [45]. The intramolecular coupling was taken as $S_c = 0.5$.

(4) *Electronic coupling.* On the basis of previous fitting analysis for τ_1 and τ_2 at $T = 300$ K, together with $\Delta G_1 = -500\ cm^{-1}$ (Section 2), we took $V_{PB} = 20\ cm^{-1}$ and $\alpha = V_{PB}/V_{PH} = 2$ [40].

(5) *Dimer internal conversion.* This surprisingly fast process, which presumably reflects the low energy gap of the dimer relative to the single bacteriochlorophyll, was taken from the experimental data $k_d = (300\ ps)^{-1}$ [69].

(6) *Recombination rates.* We have taken the experimental values $k_S = (20\ ns)^{-1}$ and $k_T = (2\ ns)^{-1}$ at $T = 300$ K, while the recombination rate of the P^+B^-H was estimated for scaling of the Franck–Condon factors for k_T and k_S to be $k_R = (1\ ns)^{-1}$.

(7) *The quinone reduction rate.* The experimental value $k_Q = (200\ ps)^{-1}$ at $T = 300$ K [13–16] was taken.

The kinetic equations were solved for each set of the parameters. ΔG_1 (and ΔG) were varied as specified in point (1) above, while all the other nuclear and electronic parameters were fixed (points (1)–(6)). The kinetic analysis resulted in three lifetimes τ_j ($j = 1$–3) and an amplitudes matrix $A_j^{(k)}$ ($j, k = 1$–3), with the temporal populations

$$[P^*](t) = \sum_{j=1}^{3} A_j^{(1)}\exp(-t/\tau_j), \quad (3.16a)$$

$$[P^+B^-H](t) = \sum_{j=1}^{3} A_j^{(2)}\exp(-t/\tau_j), \quad (3.16b)$$

$$[P^+BH^-](t) = \sum_{j=1}^{3} A_j^{(3)}\exp(-t/\tau_j). \quad (3.16c)$$

We consider now some features of the kinetics for the microscopically homogeneous model system at $T = 300$ K. Three relaxation times are exhibited (Fig. 4). For $\Delta G_1 = -500\ cm^{-1}$ (which mimics the native RC) the lifetimes τ_1 and τ_2 fit the experimental lifetime data for the ultrashort lifetimes, while τ_3 represents the quinone reduction. This agreement just provides a consistency check for the parameters used by us. Over a broad range of $\Delta G_1 = -500$ to $1500\ cm^{-1}$ the shortest lifetimes τ_2 vary only by 30% (Fig. 4). The long lifetime τ_3 also exhibits a weak

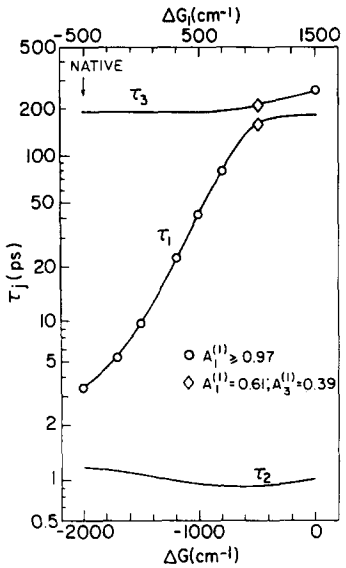

Fig. 4. The relaxation times and amplitudes for the decay of the excited dimer $^1P^*$ as function of ΔG_1 ($\Delta G_2 = -1500$ cm^{-1}) at $T = 300$ K, in the homogeneous model. The relevant parameter set is given in the legend to Fig. 3.

ΔG_1 dependence being practically constant for $\Delta G_1 = -500$ to 900 cm^{-1} and then increasing by $\sim 40\%$ towards the value of k_d^{-1}. Of considerable interest is the marked ΔG_1 dependence of τ_1 (Fig. 4), which increases with increasing ΔG_1 from $\tau_1 = 3.5$ ps at $\Delta G_1 = -500$ cm^{-1} to $\tau_1 = 186$ ps for $\Delta G_1 = 1500$ cm^{-1}. At $\Delta G_1 = 1000$ cm^{-1} a near degeneracy of the eigenvalues of the kinetic matrix is exhibited with the values of τ_1 and τ_3 being close (Fig. 4). The upper limit for the longest lifetimes (τ_1 or τ_3) of the system is given by the internal conversion time $(k_d)^{-1} = 300$ ps.

Of central interest is the time evolution of $[P^*](t)$, Eq. (3.16a). An examination of the vector $(A_1^{(1)}, A_2^{(1)}, A_3^{(1)})$ (Fig. 4) reveals that $P(t)$ is practically exponential over the entire ΔG_1 domain. For $\Delta G_1 = -500$ to 300 cm^{-1} $A_1^{(1)}$ dominates with $A_1^{(1)} > 0.98$, $A_1^{(2)}/A_1^{(1)} \leqslant 0.02$ and $A_1^{(3)}/A_1^{(1)} < 0.005$. Accordingly, $P(t)$ in a homogeneous system reveals a negligible short-time component and does not exhibit a long-time component. Increasing ΔG_1 towards $\Delta G_1 = 1000$ cm^{-1} near degeneracy of the kinetic matrix results in biexponential decay with two close lifetimes $\tau_1 = 160$ ps and $\tau_2 = 210$ ps. A further increase of ΔG_1 towards 1500 cm^{-1} exhibits a single long lifetime component for $P(t)$ with the lifetime $\tau_3 = 282$ ps with $A_1^{(1)}/A_3^{(1)} = 0.02$ (Fig. 4). Thus for the microscopically homogeneous model system $P(t)$ is represented by a single exponential over the entire relevant ΔG_1 domain, with some near degeneracy effects around $\Delta G_1 \approx 1000$ cm^{-1}. The characteristic decay time for $[P^*](t)$ is expected to exhibit a two orders of magnitude lengthening over the energy gap domain which is relevant for the effects of mutagenesis on the primary ET.

4. Kinetic heterogeneity in the parallel mechanism

The kinetic scheme has to incorporate the effects of static heterogeneity. The parallel sequential-superexchange scheme was extended by the incorporation of the energy distribution of the ion pair states P^+BH^- and P^+B^-H. Magnetic data for the recombination of P^+BH^- have established that static heterogeneity of the energy of this ion pair can be described in terms of a Gaussian distribution of the energy gap ΔG (Fig. 1) with $\sigma = 400$ cm^{-1} [56]. In order to minimize (unknown) input parameters we have taken the energy levels of the ion pairs P^+B^-H and P^+BH^- to be correlated. The energy distribution function $p(\Delta G_1')$ for the energy levels $\{\Delta G_1'\}$ around the mean value ΔG_1 for the ion pairs P^+B^-H was chosen according to a Gaussian

$$p(\Delta G_1') = (2\pi\sigma^2)^{-1/2} \times \exp\left[-(\Delta G_1' - \Delta G_1)^2/2\sigma^2\right]. \quad (4.1)$$

The same energy distribution applies to the ion pair state P^+BH^-, with energy levels

$$\Delta G' = \Delta G_1' - 1500 \text{ cm}^{-1}. \quad (4.2)$$

The energy distribution parameter was taken from the analysis of the radical pair dynamics in a magnetic field [56] as $\sigma = 400$ cm^{-1}.

Calculations were performed for room temperature $T = 300$ K, using the electronic and energetic parameters advanced in Section 3. In addition, model calculations were performed for a low temperature system at $T = 20$ K using the same parameters. We are well aware of the limitations of such a low temperature approximation, which does not account for the anisotropic contraction, which may modify

electronic, energetic and nuclear parameters. Nevertheless, such low temperature simulations will be of use for the elucidation of the gross features of the ET kinetics.

The kinetic analysis was conducted for the inhomogeneously broadened system. We calculated the lifetimes vector $\boldsymbol{\tau}(\Delta G_1') = \{\tau_j(\Delta G_1')\}$ and the amplitude matrix $\mathbf{A}(\Delta G_1') = \{A_j^{(k)}(\Delta G_1')\}$ for each value of $\Delta G_1'$ within a discretized Gaussian distribution ($\sigma =$ 400 cm^{-1}) of 800 values.

The static heterogeneity results in a distribution of the lifetimes. In Figs. 5 and 6 we present the probability density of the distribution of the decay times of $^1P^*$

$$q(\tau) = \sum_j \int d(\Delta G_1')\ \delta\big(\tau - \tau_j(\Delta G_1')\big) \times A_j^{(1)}(\Delta G_1')\, p(\Delta G_1'), \qquad (4.3)$$

versus τ. For the native RC (Fig. 5) at $T = 300$ K and at $T = 20$ K, we note that $q(\tau)$ peaks at $\sim \tau_1$, i.e., $\tau_1 = 3.5$ ps at room temperature and $\tau_1 = 1.5$ ps at $T = 20$ K, exhibiting the weak non-Arrhenius temperature dependence of the experimental nearly activationless ET. Longer time tails are exhibited with $\sim 20\%$ of the probability density for $\tau_1 \geqslant 5$ ps at room temperature, while for $T = 20$ K about 40% of the probability density is manifested for $\tau_1 \geqslant 2.5$ ps. Thus the effect of the distribution of lifetimes is considerably enhanced at low temperatures. The probability density $q(\tau)$, Eq. (4.4), for a series of model mutants with $\Delta G_1 = 0$–1500 cm^{-1} (Fig. 6) reveals broad distributions. When the temporal decay of $^1P^*$ in the homogeneous system is dominated by a single exponential (Fig. 4), $q(\tau)$ in the heterogeneous system peaks around $\sim \tau_1$. For $\Delta G_1 = -500$ cm^{-1} (native RC) to 700 cm^{-1} the distribution $q(\tau)$ is skewed towards higher values of τ (Fig. 5). For $\Delta G_1 = 1000$ cm^{-1}, when near degeneracy of the kinetic matrix prevails, a very broad distribution of $q(\tau)$ is exhibited, spanning the entire domain of τ. Finally, for the large $\Delta G_1 = 1500$ cm^{-1} the distribution of the decay times peaks around the upper limit of k_D^{-1}, being skewed towards a low value of τ.

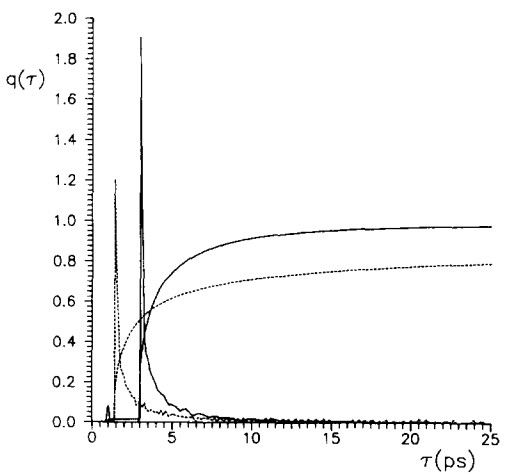

Fig. 5. The probability density $q(\tau)$, Eq. (4.8), of the $^1P^*$ relaxation time distribution for the native RC ($\Delta G = -2000$ cm^{-1}, $\Delta G_1 = -500$ cm^{-1}), and its accumulated value. (1) Solid line $T = 300$ K. (2) Dashed line $T = 20$ K.

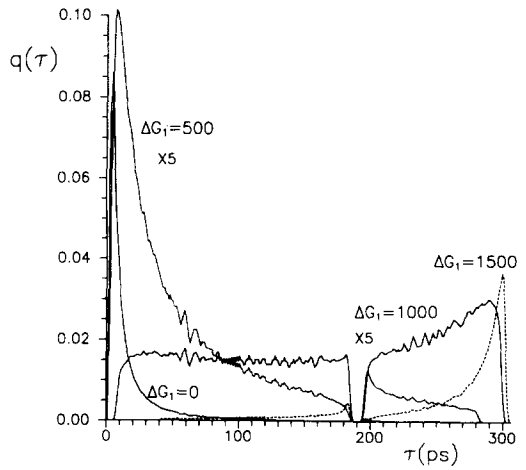

Fig. 6. The probability density $q(\tau)$ for the distribution of relaxation times of $^1P^*$ at $T = 300$ K for four values of ΔG_1 ($\Delta G_1 = 0$, 500, 1000, 1500 cm^{-1}).

The time evolution of $^1P^*$ BH in the heterogeneous system is given by

$$P(t) = \int p(\Delta G_1')[P^*](\Delta G_1';\ t)\ d(\Delta G_1'), \qquad (4.4)$$

where $[P^*](\Delta G_1';\ t)$ is calculated according to Eq. (3.16a) for the given values of $\Delta G_1'$. Making use of Eq. (4.3) the time evolution, Eq. (4.4), is given by

$$P(t) = \int d\tau\ q(\tau)\exp(-t/\tau). \qquad (4.5)$$

The time dependence of the $^1P^*$ population $P(t)$ in the heterogeneous system (Figs. 7 and 8) exhibits

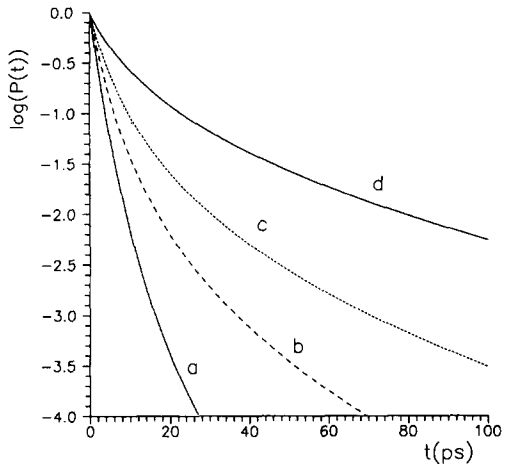

Fig. 7. Decay curves on a logarithmic scale (natural logarithm) of the $^1P^*$ population at $T = 300$ K, in the heterogeneous model: (a) $\Delta G_1 = 500$ cm^{-1}; (b) $\Delta G_1 = -200$ cm^{-1}; (c) $\Delta G_1 = 0$; (d) $\Delta G_1 = +300$ cm^{-1}.

a marked nonexponential decay. The characterization of the dispersive decay in terms of two exponentials, as empirically done [36,48], implies the representation of $q(\tau)$, Eq. (4.3), in the form $q(\tau) = B_1\delta(\tau - \bar{\tau}_1) + B_2(\tau - \bar{\tau}_2)$. We have specified the decay in terms of the lifetimes $\tau(e^{-1})$ and $\tau(e^{-2})$ for which $P(t)$ reaches the values of e^{-1} and e^{-2}, respectively. From the analysis of these lifetimes (Fig. 9), we

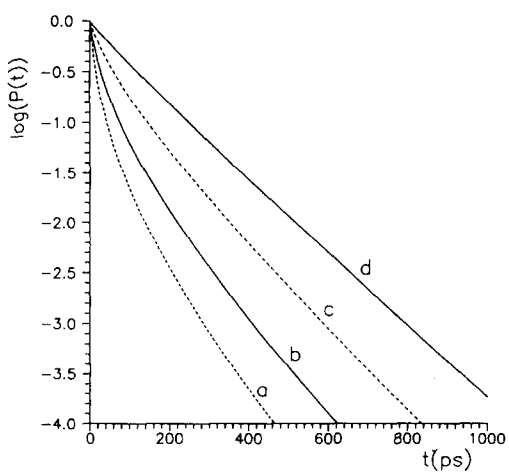

Fig. 8. Decay curves on a logarithmic scale (natural logarithm) of the $^1P^*$ population at $T = 300$ K, in the heterogeneous model: (a) $\Delta G_1 = +500$ cm^{-1}; (b) $\Delta G_1 = +700$ cm^{-1}; (c) $\Delta G_1 = +1000$ cm^{-1}; (d) $\Delta G_1 = +1500$ cm^{-1}.

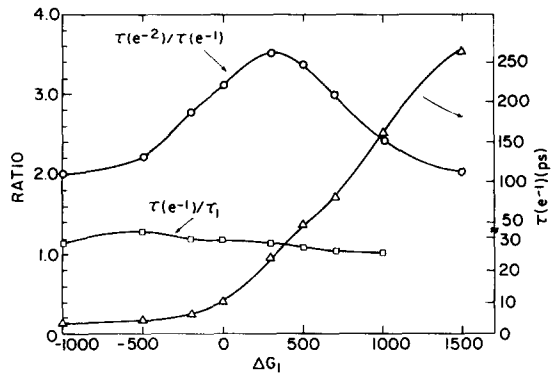

Fig. 9. Nonexponentiality of the $^1P^*$ decay in the heterogeneous model, as described in terms of the ratios of the decay times $\tau(e^{-1})/\tau_1$ and $\tau(e^{-2})/\tau(e^{-1})$. The values of $\tau(e^{-1})$ are also given.

conclude that for $\Delta G_1 = -500$ to 700 cm^{-1} the values of $\tau(e^{-1})$ in the heterogeneous system exceed by 1%–30% the values of τ_1, which dominate the decay in the homogeneous system (Fig. 4). For $\Delta G_1 = 1500$ cm^{-1}, where the decay in the homogeneous system is dominated by τ_3, $\tau(e^{-1})/\tau_3 = 0.94$. The deviation of the ratio $r = \tau(e^{-2})/\tau(e^{-1})$ from 2.00 provides a qualitative measure of the nonexponential decay. This deviation is small at the edges, i.e., $r = 2.11$ for the native RC and $r = 2.06$ for $\Delta G_1 = 1500$ cm^{-1}. The small deviation of the decay from exponentiality for $\Delta G_1 = 1500$ cm^{-1} is expected as $\Delta G_1 \gg \sigma$. The deviations from exponential decay are more marked (Fig. 9) in the intermediate range of ΔG_1 values, i.e., $\Delta G_1 = -200$ to 800 cm^{-1} peaking at $\Delta G_1 = 300$ cm^{-1}. Model calculations of the time dependence of $^1P^*$ for $\Delta G_1 = -500$ cm^{-1} (the native RC) and for $\Delta G_1 = -200$ cm^{-1} in the heterogeneous system at $T = 20$ K reveal that the effects of heterogeneity are more marked at low temperatures, as evident from the dramatic nonexponentiality and long-time tails in the decay of $^1P^*$ (Fig. 10).

To make contact with experimental reality we have calculated the quantum yield Y for charge separation

$$Y = \int k_Q[P^+BH^-](t)\,dt = k_Q \sum_{j=1}^{3} A_j^{(3)}\tau_j. \qquad (4.6)$$

In Figs. 11 and 12 we display the energy gap ΔG_1 dependence of the quantum yield for $T = 300$ K and

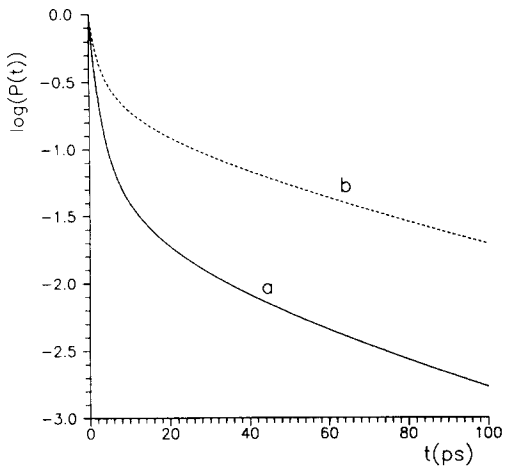

Fig. 10. Decay curves on a logarithmic scale (natural logarithm) of the $^1P^*$ population at $T = 20$ K, in the heterogeneous model: (a) $\Delta G = -2000$ cm^{-1} ($\Delta G_1 = -500$ cm^{-1}); (b) $\Delta G = -1700$ cm^{-1} ($\Delta G_1 = -200$ cm^{-1}).

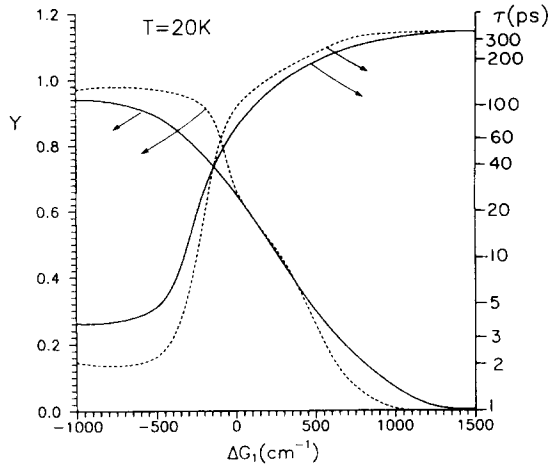

Fig. 12. The quantum yield and the relaxation time of $^1P^*$ (defined as $\tau(e^{-1})$), as function of the free energy gap ΔG_1 at $T = 20$ K. The solid line represents the Gaussian distribution around ΔG_1 ($\sigma = 400$ cm^{-1}). The dashed line represents the homogeneous model ($\sigma = 0$).

for $T = 20$ K together with the characteristic lifetimes $\tau(e^{-1})$ for the decay of $^1P^*$ in the heterogeneous system. To explore the effects of heterogeneity we have also displayed in Figs. 11 and 12 the quantum yield and the decay lifetimes of $^1P^*$ for the homogeneous system ($\sigma = 0$). The quantum yields at

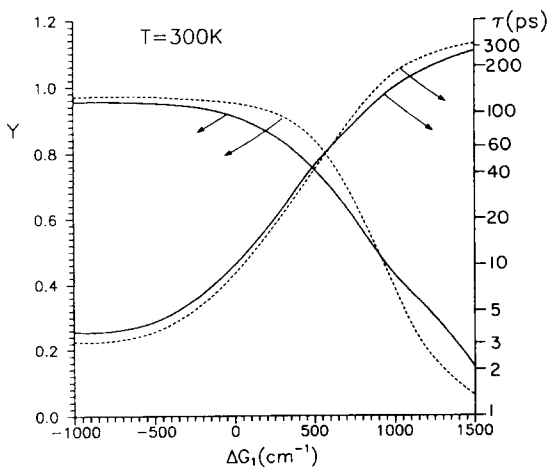

Fig. 11. The quantum yield and the relaxation time of $^1P^*$ (defined as $\tau(e^{-1})$), as function of the free energy gap ΔG_1 at $T = 300$ K. The solid line represents the Gaussian distribution around ΔG_1 ($\sigma = 400$ cm^{-1}). The dashed line represents the homogeneous model ($\sigma = 0$).

$T = 300$ K in the range $\Delta G_1 = -1000$ to 0 cm^{-1} are lower by 5%–7% from unity (due to contributions of competing channels) and exhibit a weak ΔG_1 dependence (Fig. 11). For the native RC at $T = 300$ K, $Y = 0.95$. The pioneering work of Wraight and Clayton [70], which constituted the conventional wisdom in the field, gave $Y = 1.02 \pm 0.04$ for the native RC. Recent work [71] gave [72] $Y = 0.97 \pm 0.02$ for the native RC at $T = 300$ K. Our estimate $Y = 0.95$ concurs with the experimental data [70,72]. The weak dependence of Y on ΔG_1 for $\Delta G_1 < 0$ indicates that for a large number of single site mutants the primary charge separation is efficient at room temperature. Only for mutants with $\Delta G_1 \geqslant 0$ one expects a marked reduction of Y with increasing ΔG_1 in the range where the lifetime $\tau(e^{-1})$ exceeds 20 ps or so (Fig. 11), i.e., where internal conversion competes with charge separation. The effects of heterogeneity on Y at room temperature are small for $\Delta G_1 < 0$ becoming somewhat more marked (20%) at $\Delta G_1 = 0$–500 cm^{-1}, while in the extreme case of $\Delta G_1 = 1500$ cm^{-1} the heterogeneity enhances Y by a numerical factor of 2 (Fig. 11). In general, the effects of heterogeneity on Y (Fig. 11) and on $\tau(e^{-1})$ (Figs. 8 and 11) are not marked. The rather weak manifestation of heterogeneity effects on the lifetimes provides a justification for our phenomenological analy-

sis of the experimental free energy relationships (Section 2) using the short decay component of $^1P^*$.

The energy gap dependence of the quantum yield at low temperatures $T = 20$ K (Fig. 12) is more pronounced, exhibiting a nearly linear decrease from $Y = 0.90$ for $\Delta G_1 = -500$ cm^{-1} (mimicking the native RC) to $Y = 0.20$ for $\Delta G_1 = 500$ cm^{-1}. At $\Delta G_1 = 1000$ cm^{-1} the yield further reduces to $Y = 0.1$, while photosynthetic charge separation at low temperatures is terminated for large $\Delta G_1 \geqslant 1500$ cm^{-1}. The heterogeneity effects on Y at $T = 20$ K are not pronounced for $\Delta G_1 < 500$ cm^{-1} (Fig. 12), however, for large values of $\Delta G_1 > 500$ cm^{-1} the distribution of the energy gaps considerably enhances the quantum yield for charge separation, while the decay lifetimes (which are dominated by k_d^{-1}) are only weakly affected by heterogeneity (Fig. 12).

To explore the central mechanistic issue of the interplay between the sequential and superexchange charge separation routes, we have calculated the branching ratio F_{sup} for superexchange, which is given by

$$F_{sup} = (1/Y) \sum_j \left(kA_j^{(1)} - k_- A_j^{(3)}\right)\tau_j, \qquad (4.7)$$

where the rates k and k_- are defined by Eq. (3.2). The energy gap dependence of F_{sup} (Fig. 13) is classified according to the following ranges. (I) Dominance of sequential mechanism, $F_{sup} \leqslant 0.1$. (II) Superposition of superexchange and sequential mechanisms, $0.1 < F_{sup} \leqslant 0.8$. (III) Dominance of superexchange, $F_{sup} > 0.8$. At room temperature range (I) prevails for $\Delta G_1 < 500$ cm^{-1} and only at large $\Delta G_1 = 500$–1500 cm^{-1} range (II) is realized. At $T = 300$ K, heterogeneity effects are minor in range (I), while in range (II) heterogeneity effects enhance the contribution of the sequential channel (Fig. 13). The situation is different at low temperatures for the model native RC, i.e., $\Delta G_1 = -500$ cm^{-1} at $T = 20$ K. The sequential mechanism still dominates ($F_{sup} = 0.1$), however, in the range -500 cm$^{-1} < \Delta G_1 < 500$ cm^{-1} range (II) is realized. For $\Delta G_1 > 300$ cm^{-1} range (III) is exhibited at $T = 20$ K. Finally, at very large $\Delta G_1 \geqslant 1000$ cm^{-1} $F_{sup} \approx 1.0$ and the superexchange channel exclusively dominates at $T = 20$ K, however, in this energy domain the quantum yield for charge separation is low. Finally, we note the marked effects of heterogeneity

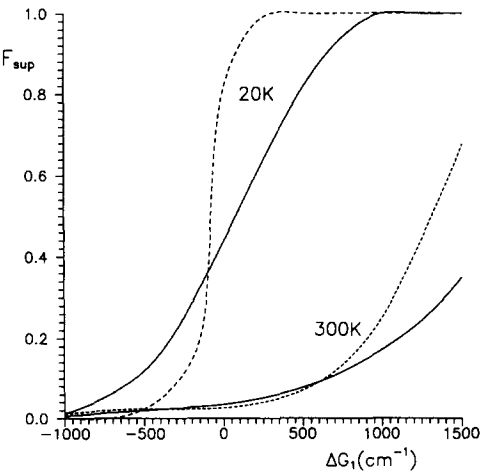

Fig. 13. The dependence of the branching ratio F_{sup} between the superexchange and the sequential rates on the (mean) energy gap ΔG_1 at $T = 300$ K and $T = 20$ K (marked on the curves). F_{sup} is expressed as the fraction of the quantum yield that originates from the superexchange channel. Dashed lines represent the results of the homogeneous model ($\sigma = 0$), while the solid lines represent the results of the heterogeneous model ($\sigma = 400$ cm^{-1}).

on F_{sup} at low temperatures. At $T = 20$ K the sharp "transition" from the sequential dominated region to the superexchange dominated region, occurring around $\Delta G_1 \approx -300$ cm^{-1} for the homogeneous system, is considerably smeared out by heterogeneity (Fig. 13).

5. Some implications of mutagenesis

The aims of our kinetic modelling are:
(1) The elucidation of the primary ET in "good" mutants (obeying rules (A) and (B) of Section 2).
(2) The characterization of some features of the temperature dependence of the primary ET.

Specific application will be given for the analysis of primary ET in the native RC, in "good" single site mutants of *R.capsulatus* and *R.sphaeroides* [36,48,62,63] and for the exploration of the gross features of the primary ET in the triple hydrogen bond mutant [LH(131) + LH(M160) + FH(197)] of the *R.sphaeroides* RC mutant [65].

From the examination of the experimental data for the "good" single site mutants [36,48,62,63] the relevant ΔG_1 scale is obtained from the redox poten-

tial scale $E_R(P^+/P) = 415$–575 mV with $E_R(P^+/P) = 495$ mV for the native RC (Fig. 3). Accordingly, $\Delta G_1 = -900$ to 300 cm^{-1} for the single site mutants. For the triple site hydrogen bond RC mutant the experimental redox potential $\Delta E_R(P^+/P) = E_R(P^+/P) - [E_R(P^+/P)](WT) \approx 2000$ cm^{-1} renders ΔG_1 to be positive and large.

The most extensive information emerges from the kinetic modelling for the native RC and its single site mutants at room temperature. The calculated ΔG_1 dependence of $\tau(e^{-1})$ exhibits a characteristic energy gap dependence (Fig. 11). The range $\Delta G_1 = -1000$ to -500 cm^{-1} corresponds to the activationless region where $\tau(e^{-1})$ varies slowly, while a strong increase of $\tau(e^{-1})$ with increasing ΔG_1 is manifested for $\Delta G_1 = -500$ to 300 cm^{-1}. The small effect of the heterogeneity on the lifetimes in the relevant ΔG_1 energy domain (Fig. 11) provides a justification for our analysis of the experimental energy gap dependence presented in Section 2. Regarding the efficiency of the charge separation, the quantum yield in the relevant range $\Delta G_1 = -900$ to 300 cm^{-1} is high, $Y = 0.95$–0.90, with Y only slightly decreasing with increasing ΔG_1. From the mechanistic point of view the charge separation for the native RC and its single site mutants is dominated by the sequential route (range (I)).

Some information emerges on the charge separation in the native RC and its single site mutants at low temperature (20 K), although these results of the simple kinetic modelling (which neglects the temperature dependence of the electronic, energetic, coupling and heterogeneity parameters) are expected to provide only general information. For the native RC at $T = 20$ K the heterogeneity effects are pronounced, e.g., $\tau(e^{-1})/\tau_1 \approx 2.6$, while the effects of heterogeneity on lifetimes of mutants with higher ΔG_1 are somewhat smaller (Fig. 12). For mutants $\tau(e^{-1})$ increases with increasing ΔG_1 (Fig. 12) exhibit a low temperature energy gap dependence. In the range $\Delta G_1 = -300$ to 300 cm^{-1}, $\tau(e^{-1})$ at 20 K is higher than the corresponding value at 300 K, so that these mutants exhibit an ordinary activated temperature dependence for the primary charge separation. The yield of the charge separation at 20 K reduces from $Y = 0.9$ for the native RC to $Y = 0.4$ for $\Delta G_1 = 300$ cm^{-1}. The role of superexchange is more pronounced at low temperatures corresponding to the coexistence of the superexchange of sequential channels (range (II)). For the native RC, where $F_{sup} \approx 0.1$ at $T = 20$ K, the contribution of superexchange originates from heterogeneity effects (Fig. 13), being manifested in the long-time tails (Fig. 10) for the decay of $P(t)$. For the single site mutants, where $F_{sup} \approx 0.1$–0.6 at $T = 20$ K, the effects of superexchange are marked.

The information which emerges from the kinetic modelling on the primary ET in the triple hydrogen bond mutant [65] is of considerable interest. We must, however, bear in mind that the experimental value of the change of the redox potential $\Delta E_R(P^+/P) = 2000$ cm^{-1} of this mutant does not necessarily correspond to $\Delta G_1 = 1500$ cm^{-1}, in view of the possible modification of the energetics of the B^-/B and H^-/H pairs by the mutation. Furthermore, other parameters (e.g., the electronic coupling, the internal conversion rate and the reorganization energy), which are taken as constants for all the mutants, may change in the triple mutant. The experimental values of the quantum yields for the charge separation in the triple mutant [65], i.e., $Y = 0.4$ at $T = 300$ K and $Y = 0.10$–0.15 at $T = 20$ K fitted well the kinetic modelling for $\Delta G_1 = 1000$ cm^{-1}. For this large value of ΔG_1 the temporal decay of $^1P^*$ does not exhibit marked deviations from exponentiality (Fig. 8) and the lifetimes $\tau(e^{-1})$ are long. The experimental lifetimes [65] are $\tau = 66$ ps at $T = 300$ K and $\tau = 290$ ps at 20 K. These results are in reasonable agreement with the lifetimes emerging from our kinetic simulations for $\Delta G_1 = 1000$ cm^{-1}, $\tau(e^{-1}) = 160$ ps for $\Delta G_1 = 1000$ cm^{-1} (while $\tau(e^{-1}) = 83$ ps for $\Delta G_1 = 700$ cm^{-1}) at $T = 300$ K and $\tau(e^{-1}) = 270$ ps for $\Delta G_1 = 1000$ cm^{-1} at 20 K. The value of $\Delta G_1 \approx 1000$ cm^{-1} extracted for the triple mutant is somewhat lower than that obtained from $\Delta E_R(P^+/P)$, however, it constitutes the largest energy gap recorded up to date for a mutant. In this triple mutant the effects of superexchange are marked ($F_{sup} \approx 0.2$) at room temperature and dominant ($F_{seq} \approx 1.0$) at low temperature.

6. Concluding remarks

In this paper we address some features of the primary ET in the RC, focusing on the energetics,

the mechanism and the effects of static heterogeneity.

Concerning the energetic of ET in the RC, we believe that current full-fledged molecular dynamics simulations [41–43] are intrinsically limited due to incomplete information on the location of water molecules and the account of long-range interactions. The phenomenological analysis of the experimental free energy relations for the native RC and its single site "good" mutants presented herein provided information for the energy gap and the reorganization energy for the primary ET. The reorganization energy $\lambda_1^0 \approx 800$ cm^{-1} is "reasonable", being lower than the reorganization energy $\lambda_T > 1300$ cm^{-1} for the recombination of the P^+BH^- ion pair [45], being comparable to reorganization energies for ET in nonpolar hydrocarbon solvents [66], and being considerably higher than the spectroscopic nuclear reorganization energy $\lambda_S = 250$ cm^{-1} for the $P \rightarrow {}^1P^*$ excitation [46,47], as expected. The low free energy gap $\Delta G_1^0(N)$ for the native RC implies the dominance of sequential ET at room temperature.

The effects of kinetic heterogeneity explored herein are of considerable interest. The manifestation of the structural heterogeneity in the primary ET rate k_1 within the RC can be traced to systems where σ is sufficiently large so that the spread in the activation energies is lower than k_BT. Accordingly, heterogeneity effects will be marked (in the classical limit) when $\sigma(\Delta G_1 + \lambda_1) > \lambda_1 k_B T$. In what follows we shall utilize the distribution parameter $\sigma = 400$ cm^{-1} [56] for both the P^+BH^- and P^+B^-H radical pairs. Marked heterogeneity effects at $T = 300$ K will be manifested when $\Delta G_1 > -300$ cm^{-1}, as is the case for many single site mutants. The most pronounced manifestation of static heterogeneity within the native RC and its single site mutants are the nonexponential temporal decay curves, which exhibit long-time tails. On the other hand, in the extreme limit, when $\Delta G_1 \gg \sigma$, the primary ET rate is slow and the internal conversion rate dominates the kinetics of ${}^1P^*$. Under these circumstances, which prevail for the triple mutant, the nonexponentiality effects of heterogeneity on $P(t)$ are less marked. A useful reduction of the experimental data suggested by our analysis involves the $\tau(e^{-1})$ lifetimes. Heterogeneity effects are small on $\tau(e^{-1})$ over the entire ΔG_1 and temperature domains and on Y for $\Delta G_1 <$ 500 cm^{-1} and over the entire temperature range. Only for very large values of $\Delta G_1 > 500$ cm^{-1} at low temperatures the effects of heterogeneity on the (low) values of Y are appreciable. The origin and nature of ET kinetic heterogeneity have still to be pursued. A recent theoretical study [73] of dispersive kinetics in the energy transfer in antenna complexes addresses the inherent glass-like structural heterogeneity in membrane proteins, and may be relevant for the problem at hand.

Regarding the mechanistic issues of the primary charge separation, our kinetic modelling has established that room temperature primary ET in the native RC and in its single site mutants is dominated by the sequential mechanism. Only the triple mutant (with $\Delta G_1 \approx 1000$ cm^{-1}) exhibits a marked contribution of the superexchange route at room temperature. At low temperatures, which are relevant for biophysical diagnosis, it appears that ET in the native RC is still dominated by the sequential route, while a small ($\sim 10\%$) superexchange contribution is manifested in the long-time decay. For single site mutations ($\Delta G_1 = -300$ to 300 cm^{-1}) at low temperatures there is an interplay between the sequential and the superexchange routes, while superexchange dominates in the triple mutant with the large $\Delta G_1 \approx$ 1000 cm^{-1} gap. Thus the biological function of the native RC of photosynthetic bacteria at room temperature is dominated by the sequential mechanism. The superexchange route enables the prevalence of primary ET in mutants with extreme values of the energy gap at room temperature and in most mutants at low temperatures. The heterogeneous parallel sequential-superexchange mechanism presented herein is of intrinsic significance to insure the stability of the primary charge separation in the RC, being stable (i.e., $Y \geqslant 0.5$) for variations of ΔG_1 over a range of 2000 cm^{-1} (6 kcal mol^{-1}). This stability of the primary ET provides a safety valve, which insures the occurrence of photosynthesis in different native and mutagenetically modified systems over a broad temperature range.

Acknowledgements

We are grateful to Professor A.P. Allen for helpful discussions and for communicating to us the results of his work prior to publication.

References

[1] J. Deisenhofer, O. Epp, K. Miki, R. Huber and H. Michel, J. Mol. Biol. 180 (1984) 385.

[2] J. Deisenhofer, O. Epp, K. Miki, R. Huber and H. Michel, Nature 318 (1985) 618.

[3] J.C. Williams, L.A. Steiner and G. Feher, Proteins 1 (1986) 312.

[4] J. Deisenhofer and H. Michel, EMBO J. 8 (1989) 2149.

[5] J.P. Allen, G. Feher, T.O. Yeates, D.C. Rees, J. Deisenhofer, H. Michel and R. Huber, Natl. Acad. Sci. USA 83 (1986) 8589.

[6] C.-H. Chang, D. Tiede, J. Tang, U. Smith, J. Norris and M. Schiffer, FEBS Letters 205 (1986) 82.

[7] T.O. Yeates, H. Komiya, A. Chirino, D.C. Rees, J.P. Allen and G. Feher, Proc. Natl. Acad. Sci. USA 85 (1988) 7993.

[8] J.P. Allen, G. Feher, T.O. Yeates, H. Komiya and D.C. Rees, Proc. Natl. Acad. Sci. USA 85 (1988) 8487.

[9] C.-H. Chang, O. El-Kabbani, D. Tiede, J. Norris and M. Schiffer, Biochemistry 30 (1991) 5352.

[10] O. El-Kabbani, C.-H. Chang, D. Tiede, J. Norris and M. Schiffer, Biochemistry 30 (1991) 5361.

[11] U. Ermler, G. Fritzch, S.K. Buchanan and H. Michel, Structure 2 (1994) 925.

[12] J. Jortner and M.E. Michel-Beyerle, in: Antennas and reaction centers of photosynthetic bacteria, ed. M.E. Michel-Beyerle (Springer, Berlin, 1985) pp. 345–354.

[13] J. Breton and A. Vermeglio, eds., The photosynthetic bacterial reaction center. Structure and dynamics (Plenum NATO ASI Series, New York, 1988).

[14] M.E. Michel-Beyerle, ed., Reaction centers of photosynthetic bacteria (Springer, Berlin, 1990).

[15] J. Breton and A. Verméglio, The photosynthetic bacterial reaction center II, NATO-ASI Series A (Life Sciences, Plenum Press, New York, 1992) Vol. 237.

[16] J. Deisenhofer and J.R. Norris, The photosynthetic reaction center (Academic Press, San Diego, 1993).

[17] N.W. Woodbury, M. Becker, D. Middenforf and W.W. Parson, Biochemistry 24 (1985) 7516.

[18] S.F. Fischer, I. Nussbaum and P.O.J. Scherer, in: Antennas and reaction centers of photosynthetic bacteria, ed. M.E. Michel-Beyerle (Springer, Berlin, 1985) p. 256.

[19] A. Ogrodnik, N. Remy-Richter, M.E. Michel-Beyerle and R. Feick, Chem. Phys. Letters 135 (1987) 576.

[20] J.R. Norris, D.E. Budil, D.M. Tiede, J. Tang, S.V. Kolaczkowski, C.H. Chang and M. Schiffer, in: Progress in photosynthetic research, Vol. 1, ed. J. Biggins (Martinus Nijhoff, Dordrecht, 1987) p. 1.4.363.

[21] M.E. Michel-Beyerle, M. Plato, J. Deisenhofer, H. Michel, M. Bixon and J. Jortner, Biochim. Biophys. Acta 932 (1988) 52.

[22] M. Bixon, J. Jortner, M. Plato and M.E. Michel-Beyerle, in: The photosynthetic bacterial reaction center. Structure and dynamics, eds. J. Breton and A. Vermeglio (Plenum NATO ASI Series, New York, 1988) p. 399.

[23] M. Plato, K. Möbius, M.E. Michel-Beyerle, M. Bixon and J. Jortner, J. Am. Chem. Soc. 110 (1988) 7279.

[24] M. Bixon, M.E. Michel-Beyerle and J. Jortner, Isr. J. Chem. 28 (1988) 155.

[25] M. Bixon, J. Jortner, M.E. Michel-Beyerle and A. Ogrodnik, Biochim. Biophys. Acta 977 (1989) 273.

[26] R.A. Friesner and Y. Won, Biochim. Biophys. Acta 977 (1989) 99.

[27] R.A. Marcus, Isr. J. Chem. 28 (1988) 205.

[28] R. Haberkorn, M.E. Michel-Beyerle and R.A. Marcus, Proc. Natl. Acad. Sci. USA 70 (1979) 4185.

[29] R.A. Marcus, Chem. Phys. Letters 133 (1987) 471.

[30] S.V. Chekalin, Ya. A. Matveetz, A.Ya. Shkuropatov, V.A. Shuvalov and A.P. Yartzev, FEBS Letters 216 (1987) 245.

[31] R.A. Marcus, Chem. Phys. Letters 146 (1977) 13.

[32] S. Creighton, J.-K. Hwang, A. Warshel, W.W. Parson and J. Norris, Biochem. 27 (1988) 774.

[33] W. Holzapfel, U. Finkele, W. Kaiser, D. Oesterhelt, H. Scheer, H.U. Stilz and W. Zinth, Chem. Phys. Letters 160 (1989) 1.

[34] W. Holzapfel, U. Finkele, W. Kaiser, D. Oesterhelt, H. Scheer, H.U. Stilz and W. Zinth, Proc. Natl. Acad. Sci. USA 87 (1990) 5168.

[35] C. Lauterwasser, U. Finkele, H. Scheer and W. Zinth, Chem. Phys. Letters 183 (1991) 471.

[36] P. Hamm, K.A. Gray, D. Oesterhelt, R. Feick, H. Scheer and W. Zinth, Biochim. Biophys. Acta 1142 (1993) 99.

[37] T. Arlt, S. Schmidt, W. Kaiser, C. Lauterwasser, M. Meyer, H. Scheer and W. Zinth, Proc. Natl. Acad. Sci. USA 90 (1993) 11757.

[38] P.M. Schmidt, T. Arlt, P. Hamm, H. Huber, T. Nägele, J. Wachtveitel, M. Meyer, H. Scheer and W. Zinth, Chem. Phys. Letters 223 (1994) 116.

[39] M. Bixon, J. Jortner and M.E. Michel-Beyerle, Biochim. Biophys. Acta 1056 (1991) 301.

[40] M. Bixon, J. Jortner and M.E. Michel-Beyerle, The photosynthetic bacterial reaction center II, NATO-ASI Series A (Life Sciences, Plenum Press, New York, 1992) Vol. 237, p. 291.

[41] W.W. Parson, Z.T. Chu and A. Warshel, Biochem. Biophys. Acta 1017 (1990) 251.

[42] M. Mercht, J.N. Gehlen, D. Chandler and M. Newton, J. Am. Chem. Soc. 115 (1993) 4178.

[43] A. Warshel, Z.T. Chu and W.W. Parson, Photochem. Photobiol. A 82 (1994) 123.

[44] M. Volk, A. Ogrodnik and M.E. Michel-Beyerle, in: Anoxygenic photosynthetic bacteria, eds. R.E. Blankenship, M.T. Medigan and C.E. Bauer (Kluwer, Dordrecht, 1995), in press.

[45] M. Bixon, J. Jortner and M.E. Michel-Beyerle, Z. Phys. Chem. 180 (1993) 193.

[46] R. Raja, S. Reddy, P.A. Lyle and G.J. Small, Photosynth. Res. 31 (1992) 167.

[47] P.A. Lyle, S. Kolaczkowski and G.J. Small, J. Phys. Chem. 97 (1993) 6924.

[48] Y. Jia, T.J. DiMagno, C.-K. Chan, Z. Wang, M. Du, D.K.

Hanson, M. Schiffer, J.R. Norris, G.R. Fleming and M.S. Popov, J. Phys. Chem. 97 (1993) 13180.
[49] M.G. Rockley, M.W. Windsor, R.J. Cogdell and W.W. Parson, Proc. Natl. Acad. Sci. USA 72 (1975) 2251.
[50] P.O.J. Scherer and S.F. Fischer, J. Phys. Chem. 93 (1989) 1633.
[51] M.A. Steffen, K. Lao and S.G. Boxer, Science 264 (1994) 810.
[52] C. Kirmaier, D. Holten and W.W. Parson, Biochim. Biophys. Acta 810 (1985) 49.
[53] C. Kirmaier and D. Holten, Proc. Natl. Acad. Sci. USA 87 (1990) 3552.
[54] M. Du, S.J. Rosenthal, X. Xie, T.J. DiMagno, M. Schmidt, D.K. Hanson, M. Schiffer, J.R. Norris and G.R. Fleming, Proc. Natl. Acad. Sci. USA 89 (1992) 8517.
[55] M.G. Müller, K. Griebenow and A.R. Hozwarth, Chem. Phys. Letters 199 (1992) 465.
[56] A. Ogrodnik, W. Nenpp, M. Volk, G. Aumeier and M.E. Michel-Beyerle, J. Phys. Chem. 98 (1994) 3432.
[57] G.J. Small, J.M. Hayes and R. Silbey, J. Phys. Chem. 96 (1992) 7499.
[58] M.H. Vos, J.C. Lambry, S.J. Robles, D.C. Youvan, J. Breton and J.L. Martin, Proc. Natl. Acad. Sci. USA 88 (1991) 8885.
[59] M.H. Vos, F. Rappaport, J.C. Lambry, J. Breton and J.L. Martin, Nature 363 (1993) 320.
[60] M.H. Vos, M.R. Jones, C.N. Hunter, J. Breton, J.C. Lambry and J.L. Martin, Biochemistry 93 (1994) 6750.
[61] M. Bixon and J. Jortner, Chem. Phys. 176 (1993) 467.
[62] J.C. Williams, R.G. Alden, H.A. Murchison, J.M. Peloquin, N.W. Woodbury and J.P. Allen, Biochemistry 31 (1992) 11029.
[63] H.A. Murchison, R.G. Alden, J.P. Allen, J.M. Peloquin, A.K.W. Taguchi, N.W. Woodbury and J.C. Williams, Biochemistry 32 (1993) 3498.
[64] V. Nagarajan, W.W. Parson, D. Davis and C.C. Schenck, Biochemistry 32 (1993) 12324.
[65] N.W. Woodbury, S. Lin, X. Lin, J.M. Peloquin, A.K.W. Taguchi, J.C. Williams and J.P. Allen, Chem. Phys; this issue, in press.
[66] M. Bixon and J. Jortner, J. Phys. Chem. 95 (1991) 1942.
[67] A. Ogrodnik, M. Volk, R. Letterer, R. Feick and M.E. Michel-Beyerle, Biochim. Biophys. Acta 936 (1988) 361.
[68] R.A. Goldstein, L. Takiff and S.G. Boxer, Biochim. Biophys. Acta 934 (1988) 253.
[69] U. Eberl, M. Gilbert, W. Keupp, T. Langenbacher, J. Siege, I. Sinning, A. Ogrodnik, S.J. Robles, J. Breton, D.C. Youvan and M.E. Michel-Beyerle, The photosynthetic bacterial reaction center II, NATO-ASI Series A (Life Sciences, Plenum Press, New York, 1992) Vol. 237, p. 253.
[70] C.A. Wraight and R.K. Clayton, Biochim. Biophys. Acta 333 (1973) 246.
[71] M. Volk, G. Scheidel, A. Ogrodnik, R. Feick and M.E. Michel-Beyerle, Biochem. Biophys. Acta 1058 (1991) 217.
[72] P. Müller, A. Ogrodnik and M.E. Michel-Beyerle, to be published.
[73] S.V. Kolaczkowski, J.M. Hayes and G.J. Small, J. Phys. Chem. 98 (1994) 13418.